



# Reduced ice number concentrations in contrails from low aromatic biofuel blends

Tiziana Bräuer<sup>1</sup>, Christiane Voigt<sup>1, 2</sup>, Daniel Sauer<sup>1</sup>, Stefan Kaufmann<sup>1</sup>, Valerian Hahn<sup>1</sup>,  
Monika Scheibe<sup>1</sup>, Hans Schlager<sup>1</sup>, Felix Huber<sup>1, 3</sup>, Patrick Le Clercq<sup>4</sup>, Richard H. Moore<sup>5</sup>, and Bruce  
E. Anderson<sup>5</sup>

<sup>1</sup>German Aerospace Center, Oberpfaffenhofen, Germany

<sup>2</sup>Johannes Gutenberg University Mainz, Mainz, Germany

<sup>3</sup>University of the Federal Armed Forces in Munich, Munich, Germany

<sup>4</sup>German Aerospace Center, Stuttgart, Germany

<sup>5</sup>NASA Langley Research Center, Hampton, Virginia, USA

**Correspondence:** Tiziana Bräuer (tiziana.braeuer@dlr.de)

**Abstract.** Sustainable aviation fuels can reduce contrail ice numbers and radiative forcing by contrail cirrus. We measured apparent ice emission indices for fuels with varying aromatic content at altitude ranges of 9.1 – 9.8 km and 11.4 – 11.6 km. Measurement data were collected during the ECLIF II/NDMAX flight experiment in January 2018. The fuels varied in both aromatic quantity and type. Between a sustainable aviation fuel blend and a reference fuel Jet A-1, a maximum reduction in apparent ice emission indices of 40% was found. We show vertical ice number and extinction distributions for three different fuels and calculate representative contrail optical depths. Optical depths of contrails (0.5 – 3 minutes in age) were reduced by 40 to 52% for a sustainable aviation fuel compared to the reference fuel. Our measurements suggest that sustainable aviation fuels result in reduced ice particle numbers, extinction coefficients, optical depth and climate impact from contrails.

## 1 Introduction

10 In recent years, the scientific knowledge about climate forcing from global aviation emissions has constantly increased. Today, we know that air traffic contributes up to 4% to anthropogenic climate forcing (Lee et al., 2021). According to Lee et al. (2021) contrail cirrus was the biggest aviation climate forcer in 2018 with  $57.4 \text{ mW m}^{-2}$ , followed by carbon dioxide emissions with  $34.3 \text{ mW m}^{-2}$  and nitrogen oxide emissions with  $17.5 \text{ mW m}^{-2}$ . Besides new propulsion and fuselage concepts to reduce fuel consumption, the use of sustainable aviation fuels (SAF) can be a solution to implement contrail mitigation. Similar to kerosene, SAF consist of molecules containing mainly carbon and hydrogen. But in contrast to the crude oil based kerosene, SAF are not dependent on fossilized carbon and some have nearly zero aromatic content. The contrails studied in this paper formed by burning blends of hydrotreated esters and fatty acids (HEFA) and kerosene. HEFA is produced through transesterification and hydrogenation of bio-based oils (Kaltschmitt and Neuling, 2018). Due to the reduced aromatic content and varied hydrocarbon types in the fuels, they have the potential to change soot emissions and microphysical contrail properties (Voigt et al., 2021).

20 The number of initial contrail ice crystals is the driving factor for the development and the climate relevant parameters of the contrail (Burkhardt et al., 2018; Unterstrasser and Gierens, 2010). Contrails are formed behind aircraft flying at altitudes above



8 km and in conditions typically colder than  $-40^{\circ}\text{C}$ . The hot engine exhaust is mixed with ambient air, which cools the exhaust plume and increases the relative humidity with respect to liquid water (Kaufmann et al., 2014). If the conditions in the exhaust exceed water saturation, the non-volatile, ultra-fine soot particles emitted by the engines serve as condensation nuclei for water droplets. The droplets immediately freeze into ice particles (Heysmsfield et al., 2010; Kärcher, 2018). The development of a line-shaped contrail is governed by the superposition of dynamic and microphysical processes and the particle and trace gas concentrations are inhomogeneously distributed. A fraction of the ice crystals follow a downward movement and form the lower primary wake. At the same time the ice crystals in the upper part of the contrail, near the flight level, grow by uptake of water and form the secondary wake. Schumann et al. (2013) showed that the ice particle concentrations are larger in the secondary wake of the contrail. Vertical profiles of one to four minutes old contrails were also analysed by Gayet et al. (2012) and Jeßberger et al. (2013) with similar results. Kleine et al. (2018) assessed the sublimation effects with data of the ECLIF I experiment and showed that both soot and ice particle number concentrations are a function of the position behind and below the contrailing aircraft.

SAF have been researched during several ground and flight experiments (Beyersdorf et al., 2014; Zschoke et al., 2012), proving that the use of jet fuels with varying properties is possible in the modern aircraft fleet. Moore et al. (2017) used in situ data to show that biofuel blending reduces soot particle number and mass emissions by 50 to 70%. A reduction in contrail ice particle numbers of similar magnitude was reported by Voigt et al. (2021) for semisynthetic and biofuel blends observed during the ECLIF I and ECLIF II/NDMAX experiments near 10 km altitude. Here, we give a more comprehensive overview of the ECLIF II/NDMAX contrail ice measurements and extend the study to a larger altitude range between 9.1 and 9.8 km. We also add observations for higher altitudes between 11.4 and 11.6 km. The influence of ambient parameters on microphysical contrail properties is discussed by Bräuer et al. (2021).

In the following, we analyse apparent ice emission indices formed from burning fuels of varying composition and also show vertical profiles of apparent ice emission indices and extinction coefficients in the young contrails. We further contribute to investigations of the contrail climate impact by deriving the individual optical depths of young contrails resulting from burning different fuels.

## 2 Experiment and instrumentation

### 2.1 ECLIF II/NDMAX

The ECLIF II/NDMAX flight experiment was part of the DLR project *Emission and Climate Impact of Alternative Fuels* and the *NASA DLR Multidisciplinary Airborne Experiment*. It aimed to quantify the impact of jet fuel aromatic content and molecular structure on soot emissions, ice crystals formation and contrail properties (Bräuer et al., 2021; Voigt et al., 2021). The experiment took place in January 2018 over northern Germany. As emissions source aircraft, the DLR A320 Advanced Technology Research Aircraft with two V2527-A5 engines was used (Figure 1). The NASA DC-8 Airborne Science Laboratory followed the A320 in a distance between 4 and 30 km (far field) and measured non-volatile particle number and mass, ice crystal number size distributions, carbon dioxide ( $\text{CO}_2$ ) and other emissions. The distances correspond to a contrail age between 30



55 seconds and three minutes. These distances are necessary to avoid saturation of the optical particle counters. The aircraft followed each other on an elongated, oval flight track at altitudes between 7.8 and 11.6 km.



**Figure 1.** Photograph of the DLR A320 with contrail in January 2018 during the ECLIF II/NDMAX flight experiment.

During ECLIF II/NDMAX airborne measurements, three different jet fuels were studied: a reference fuel Jet A-1 (Ref 3) and two blends of reference fuels and HEFA produced from camelina oil (SAF 1 and SAF 2). Relevant fuel properties are described in Table 1. By varying blending ratios, different aromatic contents were obtained in the fuels. Aromatics are cyclic hydrocarbons, characterized by conjugated double bonds. Incomplete combustion of hydrocarbons in the fuels leads to the generation of soot particles. One type of aromatics, the stable, bicyclic naphthalene molecules, are thought to increase the sooting behaviour during fuel combustion (Brem et al., 2015; Chin and Lefebvre, 1990). Therefore, SAF 1 and SAF 2 are designed to vary in their naphthalene content, while their total aromatic content is in the same range. Results of the ground measurements during ECLIF II/NDMAX are published by Schripp et al. (2021).

## 65 2.2 Particle and trace gas measurements

Ice number concentrations were measured with the Fast Forward Scattering Spectrometer Probe (FFSSP) in a particle size range between 1 and 25  $\mu\text{m}$  (Baumgardner and Gandrud, 1998). The data were corrected for small particles following Bräuer et al. (2021) so that particle concentration between 0.5 and 1  $\mu\text{m}$  can also be estimated. The instrument was mounted next to the  $\text{CO}_2$  inlet on the upper side of the DC-8 fuselage. The probe has been previously used for contrail measurements during multiple recent studies (Chauvigné et al., 2018; Gayet et al., 2012; Voigt et al., 2010, 2011), and its electronics received an update in 2017, such that the recording of single particle data is possible. The sampling area of 0.19  $\text{mm}^2$  was determined by laboratory calibrations and the instrument was size-calibrated on the basis of a T-Matrix calculation for an ice particle aspect ratio of 0.5 (Borrmann et al., 2000; Luo et al., 2003; Rosenberg et al., 2012).



**Table 1.** Properties and sample statistic of jet fuels burned during ECLIF II/NDMAX

		Sustainable Aviation Fuel 1	Sustainable Aviation Fuel 2	Reference Fuel 3	Reference Fuel 4 <sup>†</sup>
Fuel composition		51% Ref 3 + 49% HEFA	70% Ref 4 + 30% HEFA	100% Jet A-1	100% Jet A-1
Aromatics*	vol%	8.5	9.5	18.6	16.5
Naphthalenes**	mass%	0.61	0.045	1.17	0.13
Hydrogen***	mass%	14.40	14.51	13.65	14.08
H:C ratio		2.005	2.023	1.884	1.953
Sulphur****	mass%	0.007	<0.001	0.012	<0.001
Contrail samples:					
Medium altitudes		103	63	–	–
High altitudes		38	54	12	–

\*ASTM D1319, \*\*ASTM D1840, \*\*\*ASTM D7171, \*\*\*\*ISO 20884, <sup>†</sup>only probed during ground tests

CO<sub>2</sub> was measured with a commercial Picarro G1301-m greenhouse gas analyser based on wavelength-scanned cavity ring-down spectroscopy. Detailed information on the Picarro analyser can be found in Crosson (2008). Air from outside the aircraft was sampled by a backward facing inlet. Several calibrations were performed with commercial gas standards. Accuracy depends on the cell pressure of the instrument and its temperature during operation (peak broadening). Data are corrected for water vapour content following Rella et al. (2013). The time delay of the gas flow on the way from the inlet to the measurement cell was estimated to be 3.3 s.

### 3 Calculation of hydrogen to carbon ratio, emission index and extinction coefficient

Kerosene contains mainly carbon, hydrogen and sulphur. It can be assumed that the sulphur content is negligible (in general less than 0.07 mass%) and therefore the hydrogen to carbon (H:C) mole fraction ratio can be calculated for the known mass fraction of hydrogen  $w_H$  as followed:

$$\frac{x_H}{x_C} = \frac{\frac{w_H}{M_H}}{\frac{100 \text{ mass}\% - w_H}{M_C}} \quad (1)$$

Environmental conditions, instabilities in the trailing vortices and dilution lead to spatial inhomogeneities in the exhaust (Schumann et al., 2017; Unterstrasser, 2016). Therefore, the particle concentrations in an aircraft plume are normalized by CO<sub>2</sub> as a proxy for fuel burn in order to calculate an emission indices (EI). The ice number concentrations are related to the mass of fuel burnt by scaling the measurements to the fuel-dependent CO<sub>2</sub> emission index. For this calculation, we assume that the combustion system has 100% fuel conversion efficiency. As ice particles are not directly emitted by the engines, the term apparent ice particle emission index is used. Emission indices are calculated following Moore et al. (2017).



The individual impact of a contrail on radiation through the atmosphere depends on the extinction properties of the ice crystals. The extinction coefficients depend on the extinction efficiencies, the projected area of the ice particles and the number concentration (Schumann et al., 2011). The extinction efficiencies were calculated for an aspect ratio of 1.0 and a wavelength of 550 nm and approach a value of 2 for large ice particles.

## 95 4 Results and discussion

### 4.1 Fuel-dependent apparent ice emission indices

As shown in Bräuer et al. (2021), temperatures near the contrail formation threshold temperature prevail when contrails are formed at altitudes below 9 km, leading to an incomplete activation of soot particles into water (Kärcher and Voigt, 2017). At these low altitudes, even small temperature variations under 1 K significantly change the particle activation fraction and the ice number concentrations in the contrails. Therefore, we concentrate our study on altitudes above 9 km. Voigt et al. (2021) showed a subset of the data at 9.1 to 9.8 km altitude, restricted to fuel flows of  $1100 \pm 100 \text{ kg h}^{-1}$  and relative humidity larger than 108%. Here, we use the complete data set for the fuel intercomparison and discuss the resulting impact and limitations.

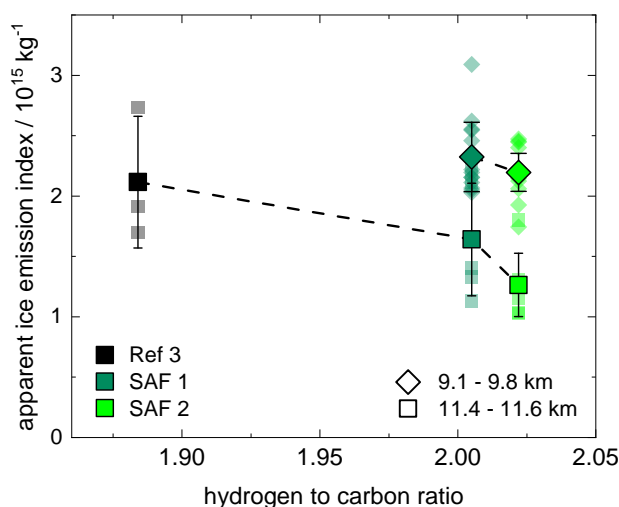


**Figure 2.** Apparent ice emission indices with respect to the hydrogen to carbon (H:C) ratio of the fuels at two different flight altitudes. H:C ratio of Ref 3 (black): 1.884, SAF 1 (dark green): 2.005, SAF 2 (light green): 2.022. Small symbols show upper 15% of the single plume encounters.

To present ice crystal number in contrails independent of contrail age, thrust level and dilution, we calculate apparent ice emission indices (AEI). In Figure 2, AEI are compared on the basis of the hydrogen to carbon (H:C) ratio of the varying fuels. For the contrails measured during ECLIF II/NDMAX (age between 30 seconds and three minutes), sublimation effects can affect the ice numbers in the vortex phase and have to be excluded to receive a climate-relevant value for AEI. Therefore, we follow Bräuer et al. (2021) and calculate the mean of the upper 15% AEI. To ensure only contrails with full soot activation



are considered, relative humidity with respect to ice is restricted to larger than 100% for altitudes between 9.1 and 9.8 km and larger than 120% for altitudes between 11.4 and 11.6 km.

110 For high altitudes, we report a 23% reduction in apparent ice emission indices when burning SAF 1 compared to Ref 3 and a reduction of 40% when burning SAF 2. For altitudes between 9.1 and 9.8 km, a 6% reduction is achieved when burning SAF 2 compared to SAF 1. These values are in general agreement with previous observations. Voigt et al. (2021) find AEI reductions in the range of 50 to 70%, when comparing to a different Jet A-1 reference fuel with lower hydrogen content. It can be stated, that the number of ice crystals is reduced through the reduction of fuel aromatic content, which is also monitored by  
115 an increase in fuel hydrogen content. Changes in fuel polycyclic aromatic composition can further increase the reductions.

#### 4.2 Vertical profiles of contrail properties

Figure 3 shows the vertical profiles of AEI (a and b) and the extinction coefficients (c and d) for the contrails resulting from burning each of the assessed fuels. The flight altitude of the A320 is the reference level and corresponds to 0 m vertical displacement on the y-axes of the figures. For reasons of simplicity, the mean values of several plume encounters are calculated  
120 in 30 m altitude sections. Because of the reduced number of plume encounters for the reference fuel Ref 3, sections with a depth of 60 m are calculated for this fuel. Due to unfavourable weather conditions, we were unable to observe contrails resulting from burning Ref 3 at flight altitudes between 9.1 and 9.8 km. The number of plume encounters per altitude and fuel type can be found in Table 1.

The vertical profiles of AEI in Figure 3a and b show typical distributions for the aircraft type A320 (Jeßberger et al., 2013; 125 Kleine et al., 2018; Schumann et al., 2013). The measurements are distributed over a vertical range of 60 m above and up to 240 m beneath the reference level of the aircraft. The physical depth of a contrail varies with ambient conditions such as atmospheric stability and the humidity distribution. Produced by the same aircraft and at the same flight altitude in similar conditions, the physical depth should be constant for varying fuels, even though in theory, different particle sizes lead to variations in sedimentation and sublimation processes (Kleine et al., 2018; Unterstrasser and Görsch, 2014).

130 Sublimation effects, which lead to a decrease of the ice crystal numbers in vertical direction below the A320, depend on the relative humidity over ice, temperature and atmospheric stability. Figure 4 shows two image recordings of the DC-8 forward camera during ECLIF II/NDMAX. Figure 4a shows a contrail unaffected by sublimation and Figure 4b shows a contrail strongly affected by sublimation with a secondary wake forming above the descending contrail vortices. In Figure 3a and b, sublimation effects of different emphasis can be observed in the vertical profiles of AEI. For both altitudes, AEI are increased at the level of the secondary wake near the initial emission level at 0 m. For altitudes between 9.1 and 9.8 km, AEI are also slightly  
135 increased in the lower primary wake and sublimation effects are reduced at these altitudes. However, the highest AEI are always found in the upper secondary wake as also shown by Kleine et al. (2018). Mean values of AEI are depicted by dashed, vertical lines and in contrast to mean AEI in Figure 2, these values consider all sublimation effects. At altitudes between 9.1 and 9.8 km the mean AEI is  $1.3 \cdot 10^{15} \text{ kg}^{-1}$  for SAF 1 and  $7.4 \cdot 10^{14} \text{ kg}^{-1}$  for SAF 2. The mean AEI at altitudes between 11.4 and 11.6  
140 km is  $5.9 \cdot 10^{14} \text{ kg}^{-1}$  for SAF 1,  $5.8 \cdot 10^{14} \text{ kg}^{-1}$  for SAF 2 and  $1.2 \cdot 10^{15} \text{ kg}^{-1}$  for Ref 3.

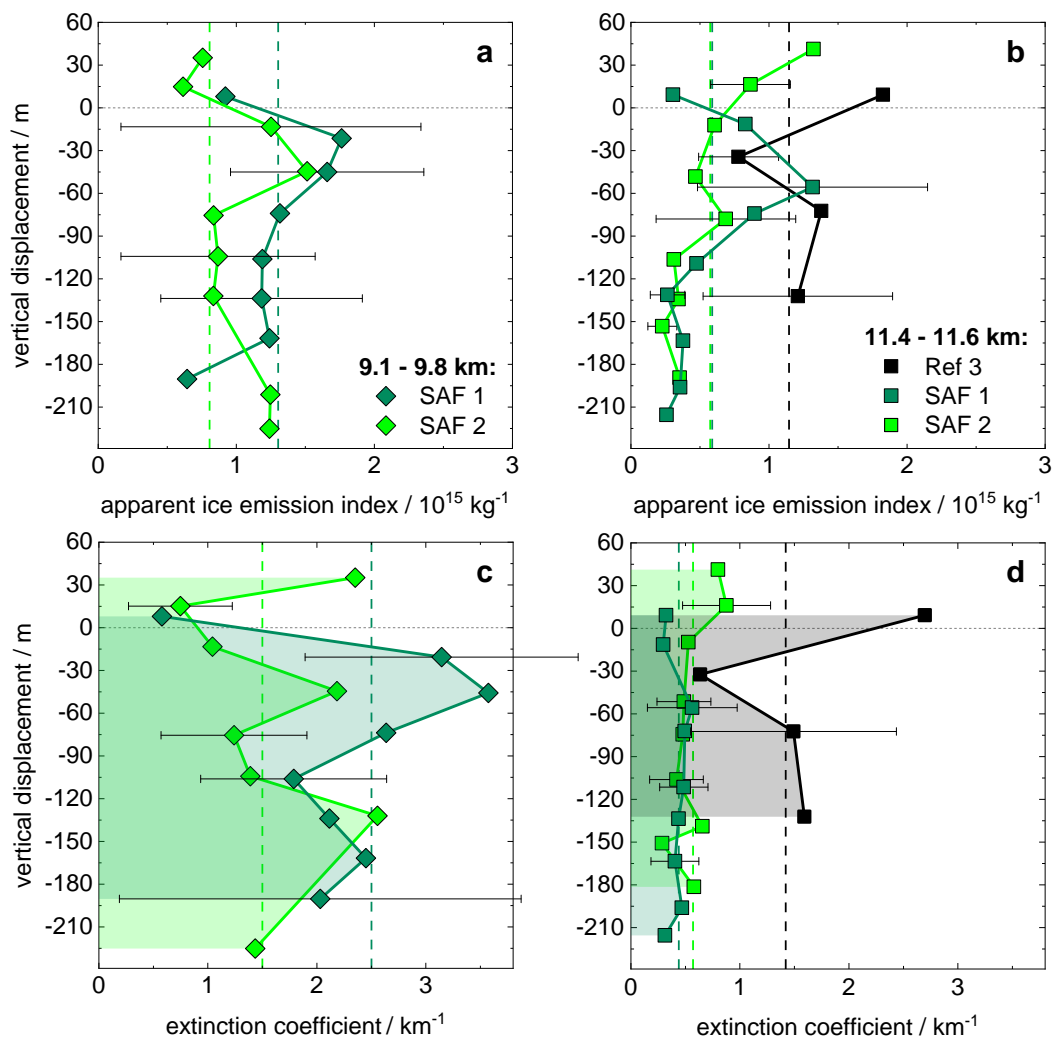


**Figure 3.** Profiles of mean AEI (a and b) and mean extinction coefficients (c and d) in 30 m sections (60 m for Ref 3). The A320 flight level is depicted by the grey, horizontal reference line at 0 m. Dashed, vertical lines show overall means. (a and c) 9.1 - 9.8 km (diamonds). (b and d) 11.4 - 11.6 km (squares).

The global climate impact of contrails is non-linearly dependent on the reduction of initial ice crystal numbers (Burkhardt et al., 2018). The dependence of contrail microphysical and radiative properties on initial ice crystal numbers then remains over the contrail cirrus life cycle. We calculate the extinction coefficients of the contrails to present the relation between contrail ice crystals and radiation. Unterstrasser and Gierens (2010) show that extinction is a suitable variable for comparing similar aged contrails. The contrail life cycle further depends on meteorological parameters like temperature and humidity, vertical wind



shear, atmospheric stability, the depth of the supersaturated layer in which the contrails are formed and the radiation budget (Unterstrasser et al., 2017; Schumann and Heymsfield, 2017).

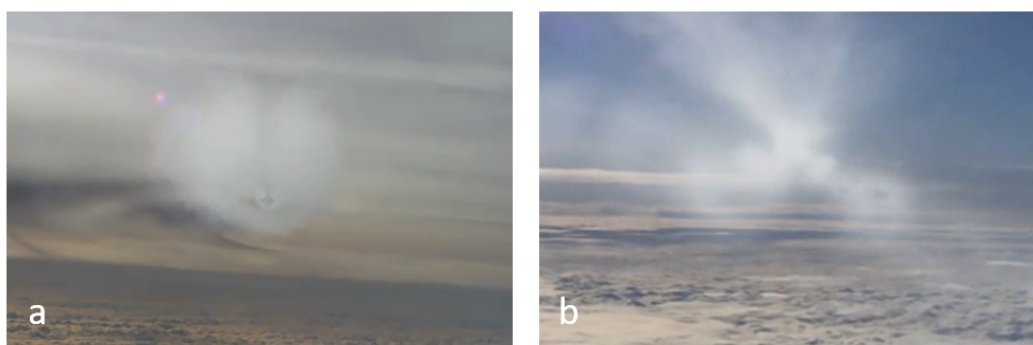


**Figure 4.** Contrails recorded by the DC-8 forward camera at different ambient conditions during ECLIF II/NDMAX.

The vertical profiles of the extinction coefficients are shown in Figure 3c and d. At altitudes between 9.1 and 9.8 km the mean extinction coefficients are  $2.5 \text{ km}^{-1}$  for SAF 1 and  $1.5 \text{ km}^{-1}$  for SAF 2. The mean extinction coefficients at altitudes  
150 between 11.4 and 11.6 km are  $0.4 \text{ km}^{-1}$  for SAF 1 and  $0.6 \text{ km}^{-1}$  for SAF 2. The mean Ref 3 extinction coefficient at the altitude between 11.4 and 11.6 km is  $1.5 \text{ km}^{-1}$  and hence a factor of 2.5 higher than the mean extinction coefficients of both biofuels at the same altitude. In a next step the extinction coefficients are used to calculate the fuel-dependent contrail optical depths in the following section.

### 4.3 Fuel-dependent contrail optical depth

155 The contrail optical depth (COD) is a dimensionless measure of the degradation that a beam of radiation directed straight downwards experiences when passing through a contrail (Wallace and Hobbs, 2006). It is derived by integrating the extinction with respect to the vertical physical contrail depth. The ECLIF II/NDMAX CODs for the measured fuels are calculated by integration of the extinction coefficients shown in Figure 3c and d (coloured areas). The calculated CODs for the three fuels at two different altitudes are presented in Figure 5. The variability bars are estimated based on the distribution of the measurements  
160 over the vertical range and reflect the uncertainties in the physical depths of the contrails. Fewer plume encounters were made for the Ref 3 fuel, which results in large variability bars.

For high altitudes, a COD reduction of 40 to 52% can be calculated when comparing the biofuel blends to the reference fuel. Due to atmospheric variability, it is not possible to evaluate the tendencies of the contrail optical depth that result from the sustainable aviation fuels. SAF 2 with reduced naphthalene content produces reduced AEI compared to SAF 1. But when  
165 calculating the climate relevant parameter of optical depth during this early contrail age, the differences are reduced or even reversed. The reason is, that reduced particle numbers under similar contrail formation conditions, will lead to larger particles, as there is more water vapour available for particle growth. The ice particle sizes are in the further contrail evolution strongly influenced by atmospheric conditions and therefore, they are highly variable. The total contrail extinction (Unterstrasser and





Gierens, 2010; Unterstrasser and GörSCH, 2014) and the radiative forcing of contrail cirrus (Burkhardt et al., 2018) are strongly  
170 dependent on initial ice crystal numbers. The optical depth varies strongly during the life cycle of a contrail (Unterstrasser and  
Gierens, 2010; Vázquez-Navarro et al., 2015).

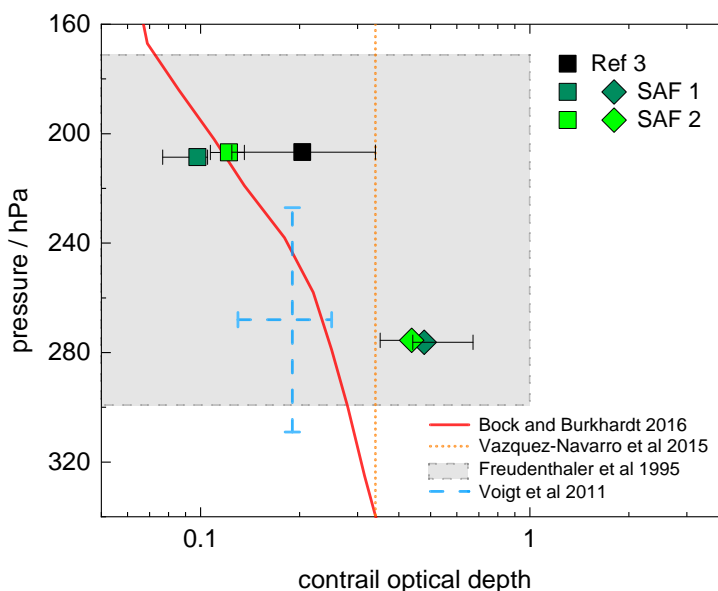


**Figure 5.** Individual contrail optical depths determined from observations and models. For the ECLIF II/NDMAX data the optical depths of contrails from the three fuels are distinguished by color and the altitudes by symbol.

In Figure 5, the calculated COD are compared with in situ and satellite observations (dashed and dotted lines) and model-derived values (compact lines). Freudenthaler et al. (1995) detected contrail height and width with a ground-based scanning lidar and Schumann et al. (2017) calculated the corresponding COD values. Results covered a COD range of 0.05 to 1 for  
175 contrail ages between 1 and 60 minutes. Voigt et al. (2010, 2011) determined optical depths of up to 6 minutes old contrails by in situ measurements. Data of the 2008 CONCERT experiment were used to derive the optical depth by multiplying the extinction with physical contrail depths calculated using dynamic vortex simulations by Holzäpfel (2006). Vázquez-Navarro et al. (2015) detected contrails with an automatic contrail tracking algorithm (ACTA) from Meteosat observations. The mean optical thickness of contrails with a mean duration of 1 h was 0.34. Finally, Bock and Burkhardt (2016) used a contrail cirrus  
180 parameterisation developed for the ECHAM5 model to describe the mean optical depth of contrails 7.5 minutes after formation with optical depth greater than 0.05 between 30 and 70°N in a vertical profile in rough agreement with the observations. Larger COD at the lowest altitudes result from neglecting incomplete contrail activation near the contrail formation temperature and have been changed in subsequent studies (Bock and Burkhardt, 2019; Burkhardt et al., 2018).

The variation of values shows the variability in individual contrail radiative impact. Different averaging volumes and a larger  
185 contrail age of 7.5 minutes in the simulation, with respect to 1-2 minutes of the observations, might explain lower COD in the global model contrails compared to the observations.



For contrail optical depths (COD) smaller than 1, the contrail radiative forcing is proportional to COD (Meerkötter et al., 1999). Lee et al. (2021) give a consolidated estimate of contrail cirrus effective radiative forcing of  $57.4 \text{ mW m}^{-2}$ . The estimations are based on several global climate models (Burkhardt and Kärcher, 2011; Bock and Burkhardt, 2016; Chen and Gettelman, 2013; Schumann et al., 2015; Bickel et al., 2020). A study by Gettelman et al. (2021) calculates a similar effective contrail radiative forcing of  $62 \text{ mW m}^{-2}$ . Uncertainties for these values are high, inter alia, because the COD remains highly uncertain (Schumann et al., 2021a, b). Sanz-Morère et al. (2020) state that global estimations of average COD can vary from 0.065 to 0.3. The individual COD of ECLIF II/NDMAX are slightly higher than the underlying COD values of the current best effective radiative forcing estimate in Lee et al. (2021), which can be explained by the early development stage of the ECLIF II/NDMAX contrails.

## 5 Conclusions and outlook

For ECLIF II/NDMAX, up to 40% reduction in apparent ice emission indices was measured. SAF 1 and 2 had similar aromatic content but varied in aromatic type. An additional reduction in AEI of up to 20% was measured for the SAF with reduced naphthalene content. The individual contrail optical depth was reduced between 40–52% for a sustainable aviation fuel compared to the reference fuel. For the future, a drastic reorientation of fuel compositions could provide strong benefits for climate, which comes without the cost of enhanced  $\text{CO}_2$  emissions when rerouting air traffic. Significant reduction of aviation climate forcing can be achieved by the widespread implementation of SAF blends in airport fuelling systems and by the use of unblended sustainable aviation fuels or even hydrogen fuels.

*Data availability.* The data are collected at the NASA data repository at <https://science-data.larc.nasa.gov/aero-fp/projects/>.

*Author contributions.* C.V., H.S., P.L. and B.A. planned the flight experiment; P.L. designed and organised the fuels; T.B., C.V., D.S., S.K., V.H., M.S., H.S., F.H., R.M. and B.A. performed the in-flight measurements, analysed the data and commented on the manuscript; T.B. performed the contrail ice data evaluation and wrote the paper. All authors contributed to the manuscript.

*Competing interests.* The authors declare that they have no conflict of interest.

*Acknowledgements.* T. B. and C. V. acknowledge funding by the Helmholtz Association under contract W2/W3-60. C. V. acknowledges funding by the German Research Foundation for SPP HALO 1294 and project VO 1504/7-1.



## References

- Baumgardner, D. and Gandrud, B. E.: A comparison of the microphysical and optical properties of particles in an aircraft contrail and mountain wave cloud, *Geophys. Res. Lett.*, 25, 1129–1132, <https://doi.org/10.1029/98GL00035>, 1998.
- Beyersdorf, A. J., Timko, M. T., Ziemba, L. D., Bulzan, D., Corporan, E., Herndon, S. C., Howard, R., Miake-Lye, R., Thornhill, K. L., Winstead, E., Wey, C., Yu, Z., and Anderson, B. E.: Reductions in aircraft particulate emissions due to the use of Fischer–Tropsch fuels, *Atmos. Chem. Phys.*, 14, 11–23, <https://doi.org/10.5194/acp-14-11-2014>, 2014.
- Bickel, M., Ponater, M., Bock, L., Burkhardt, U., and Reineke, S.: Estimating the Effective Radiative Forcing of Contrail Cirrus, *J. Clim.*, 33, 1991–2005, <https://doi.org/10.1175/JCLI-D-19-0467.1>, 2020.
- Bock, L. and Burkhardt, U.: Reassessing properties and radiative forcing of contrail cirrus using a climate model, *J. Geophys. Res. Atmos.*, 121, 9717–9736, <https://doi.org/10.1002/2016JD025112>, 2016.
- Bock, L. and Burkhardt, U.: Contrail cirrus radiative forcing for future air traffic, *Atmos. Chem. Phys.*, 19, 8163–8174, <https://doi.org/10.5194/acp-19-8163-2019>, 2019.
- Borrmann, S., Luo, B., and Mishchenko, M.: Application of the T-Matrix method to the measurement of aspherical (ellipsoidal) particles with forward scattering optical particle counters, *J. Aerosol Sci.*, 31, 789–799, 2000.
- Brem, B. T., Durдина, L., Siegerist, F., Beyerle, P., Bruderer, K., Rindlisbacher, T., Rocci-Denis, S., Andac, M. G., Zelina, J., Penanhoat, O., and Wang, J.: Effects of Fuel Aromatic Content on Nonvolatile Particulate Emissions of an In-Production Aircraft Gas Turbine, *Environ. Sci. Technol.*, 49, 13 149–13 157, <https://doi.org/10.1021/acs.est.5b04167>, PMID: 26495879, 2015.
- Bräuer, T., Voigt, C., Sauer, D., Kaufmann, S., Hahn, V., Scheibe, M., Schlager, H., Diskin, G. S., Nowak, J. B., DiGangi, J. P., Huber, F., Moore, R. H., and Anderson, B. E.: Airborne Measurements of Contrail Ice Properties - Dependence on Temperature and Humidity, *Geophys. Res. Lett.*, <https://doi.org/10.1029/2020GL092166>, 2021.
- Burkhardt, U. and Kärcher, B.: Global radiative forcing from contrail cirrus, *Nat. Clim. Chang.*, 1, 54–58, <https://doi.org/10.1038/nclimate1068>, 2011.
- Burkhardt, U., Bock, L., and Bier, A.: Mitigating the contrail cirrus climate impact by reducing aircraft soot number emissions, *NPJ Clim. Atmos. Sci.*, 1, 37, <https://doi.org/10.1038/s41612-018-0046-4>, 2018.
- Chauvigné, A., Jourdan, O., Schwarzenboeck, A., Gourbeyre, C., Gayet, J. F., Voigt, C., Schlager, H., Kaufmann, S., Borrmann, S., Mollerer, S., Minikin, A., Jurkat, T., and Schumann, U.: Statistical analysis of contrail to cirrus evolution during the Contrail and Cirrus Experiment (CONCERT), *Atmos. Chem. Phys.*, 18, 9803–9822, <https://doi.org/10.5194/acp-18-9803-2018>, 2018.
- Chen, C.-C. and Gettelman, A.: Simulated radiative forcing from contrails and contrail cirrus, *Atmos. Chem. Phys.*, 13, 12 525–12 536, <https://doi.org/10.5194/acp-13-12525-2013>, 2013.
- Chin, J. S. and Lefebvre, A. H.: Influence of Fuel Chemical Properties on Soot Emissions from Gas Turbine Combustors, *Combust. Sci. Technol.*, 73, 479–486, <https://doi.org/10.1080/00102209008951664>, 1990.
- Crosson, E. R.: A cavity ring-down analyzer for measuring atmospheric levels of methane, carbon dioxide, and water vapor, *Appl. Phys. B*, 92, 403–408, <https://doi.org/10.1007/s00340-008-3135-y>, 2008.
- Freudenthaler, V., Homburg, F., and Jäger, H.: Contrail observations by ground-based scanning lidar: Cross-sectional growth, *Geophys. Res. Lett.*, 22, 3501–3504, <https://doi.org/10.1029/95GL03549>, 1995.



- Gayet, J.-F., Shcherbakov, V., Voigt, C., Schumann, U., Schäuble, D., Jessberger, P., Petzold, A., Minikin, A., Schlager, H., Dubovik, O., ,  
and Lapyonok, T.: The evolution of microphysical and optical properties of an A380 contrail in the vortex phase, *Atmos. Chem. Phys.*,  
12, 6629–6643, 2012.
- 250 Gettelman, A., Chen, C.-C., and Bardeen, C. G.: The Climate Impact of COVID19 Induced Contrail Changes, *Atmos. chem. phys. discuss.*,  
2021, 1–17, <https://doi.org/10.5194/acp-2021-210>, 2021.
- Heymsfield, A., Baumgardner, D., DeMott, P., Forster, P., Gierens, K., and Kärcher, B.: Contrail Microphysics, *Bull. Am. Meteorol. Soc.*,  
91, 465–472, <https://doi.org/10.1175/2009BAMS2839.1>, 2010.
- Holzäpfel, F.: Probabilistic Two-Phase Aircraft Wake-Vortex Model: Further Development and Assessment, *J. Aircr.*, 43, 700–708,  
<https://doi.org/10.2514/1.16798>, 2006.
- 255 Jeßberger, P., Voigt, C., Schumann, U., Sölch, I., Schlager, H., Kaufmann, S., Petzold, A., Schaeuble, D., and Gayet, J.-F.: Aircraft type  
influence on contrail properties, *Atmos. Chem. Phys.*, 13, <https://doi.org/10.5194/acp-13-11965-2013>, 2013.
- Kaltschmitt, M. and Neuling, U., eds.: *Biokerosene - Status and Prospects*, Springer-Verlag Berlin Heidelberg, <https://doi.org/10.1007/978-3-662-53065-8>, 2018.
- 260 Kaufmann, S., Voigt, C., Jeßberger, P., Jurkat, T., Schlager, H., Schwarzenboeck, A., Klingebiel, M., and Thornberry, T.: In situ measurements  
of ice saturation in young contrails, *Geophys. Res. Lett.*, 41, 702–709, <https://doi.org/10.1002/2013GL058276>, 2014.
- Kleine, J., Voigt, C., Sauer, D., Schlager, H., Scheibe, M., Jurkat-Witschas, T., Kaufmann, S., Kärcher, B., and Anderson,  
B. E.: In Situ Observations of Ice Particle Losses in a Young Persistent Contrail, *Geophys. Res. Lett.*, 45, 13,553–13,561,  
<https://doi.org/10.1029/2018GL079390>, 2018.
- Kärcher, B.: Formation and radiative forcing of contrail cirrus, *Nat. Commun.*, 9, 1824, <https://doi.org/10.1038/s41467-018-04068-0>, 2018.
- 265 Kärcher, B. and Voigt, C.: Susceptibility of contrail ice crystal numbers to aircraft soot particle emissions, *Geophys. Res. Lett.*, 44, 8037–  
8046, <https://doi.org/10.1002/2017GL074949>, 2017.
- Lee, D., Fahey, D., Skowron, A., Allen, M., Burkhardt, U., Chen, Q., Doherty, S., Freeman, S., Forster, P., Fuglestedt, J., Get-  
telman, A., De León, R., Lim, L., Lund, M., Millar, R., Owen, B., Penner, J., Pitari, G., Prather, M., Sausen, R., and Wilcox,  
L.: The contribution of global aviation to anthropogenic climate forcing for 2000 to 2018, *Atmospheric Environ.*, p. 117834,  
270 <https://doi.org/10.1016/j.atmosenv.2020.117834>, 2021.
- Luo, B. P., Voigt, C., Fueglistaler, S., and Peter, T.: Extreme NAT supersaturations in mountain wave ice PSCs: A clue to NAT formation, *J.*  
*Geophys. Res. Atmos.*, 108, <https://doi.org/10.1029/2002JD003104>, 2003.
- Meerkötter, R., Schumann, U., Minnis, P., Doelling, D. R., Nakajima, T., and Tsushima, Y.: Radiative forcing by contrails, *Ann. Geophys.*,  
17, 1080–1094, <https://doi.org/10.1007/s00585-999-1080-7>, 1999.
- 275 Moore, R. H., Thornhill, K. L., Weinzierl, B., Sauer, D., D’Ascoli, E., Kim, J., Lichtenstern, M., Scheibe, M., Beaton, B., Beyersdorf, A. J.,  
Barrick, J., Bulzan, D., Corr, C. A., Crosbie, E., Jurkat, T., Martin, R., Riddick, D., Shook, M., Slover, G., Voigt, C., White, R., Winstead,  
E., Yasky, R., Ziemba, L. D., Brown, A., Schlager, H., and Anderson, B. E.: Biofuel blending reduces particle emissions from aircraft  
engines at cruise conditions, *Nature*, 543, 411–415, <https://doi.org/10.1038/nature21420>, 2017.
- Rella, C. W., Chen, H., Andrews, A. E., Filges, A., Gerbig, C., Hatakka, J., Karion, A., Miles, N. L., Richardson, S. J., Steinbacher, M.,  
280 Sweeney, C., Wastine, B., and Zellweger, C.: High accuracy measurements of dry mole fractions of carbon dioxide and methane in humid  
air, *Atmos. Meas. Tech.*, 6, 837–860, <https://doi.org/10.5194/amt-6-837-2013>, 2013.



- Rosenberg, P. D., Dean, A. R., Williams, P. I., Dorsey, J. R., Minikin, A., Pickering, M. A., and Petzold, A.: Particle sizing calibration with refractive index correction for light scattering optical particle counters and impacts upon PCASP and CDP data collected during the Fennec campaign, *Atmos. Meas. Tech.*, 5, 1147–1163, <https://doi.org/10.5194/amt-5-1147-2012>, 2012.
- 285 Sanz-Morère, I., Eastham, S. D., Allroggen, F., Speth, R. L., and Barrett, S.: Effect of contrail overlap on radiative impact attributable to aviation contrails, *Atmos. Chem. Phys.*, pp. 1–62, 2020.
- Schripp, T., Anderson, B., LeClercq, P., Bauder, U., Corbin, J., Smallwood, G., Lobo, P., Crosbie, E. E., Shook, M., Miake-Lye, R., Yu, Z., Freedman, A., Whitefield, P. D., Robinson, C. E., Achterberg, S. L., Köhler, M., Oßwald, P., Grein, T., Sauer, D., and Voigt, C.: Aircraft Engine Particulate Matter and Gaseous Emissions from Sustainable Aviation Fuels: Results from Ground-based Measurements during the NASA/DLR Campaign ECLIF2/ND-MAX, Elsevier Fuel, in preparation, 2021.
- 290 Schumann, U. and Heymsfield, A. J.: On the Life Cycle of Individual Contrails and Contrail Cirrus, *Meteorol Monogr.*, 58, 3.1 – 3.24, <https://doi.org/10.1175/AMSMONOGRAPHS-D-16-0005.1>, 2017.
- Schumann, U., Mayer, B., Gierens, K., Unterstrasser, S., Jessberger, P., Petzold, A., Voigt, C., and Gayet, J.-F.: Effective Radius of Ice Particles in Cirrus and Contrails, *J. Atmos. Sci.*, 68, 300–321, <https://doi.org/10.1175/2010JAS3562.1>, 2011.
- 295 Schumann, U., Jeßberger, P., and Voigt, C.: Contrail ice particles in aircraft wakes and their climatic importance, *Geophys. Res. Lett.*, 40, 2867–2872, <https://doi.org/10.1002/grl.50539>, 2013.
- Schumann, U., Penner, J. E., Chen, Y., Zhou, C., and Graf, K.: Dehydration effects from contrails in a coupled contrail–climate model, *Atmos. Chem. Phys.*, 15, 11 179–11 199, <https://doi.org/10.5194/acp-15-11179-2015>, 2015.
- Schumann, U., Baumann, R., Baumgardner, D., Bedka, S. T., Duda, D. P., Freudenthaler, V., Gayet, J.-F., Heymsfield, A. J., Minnis, P., 300 Quante, M., Raschke, E., Schlager, H., Vázquez-Navarro, M., Voigt, C., and Wang, Z.: Properties of individual contrails: a compilation of observations and some comparisons, *Atmos. Chem. Phys.*, 17, 403–438, <https://doi.org/10.5194/acp-17-403-2017>, 2017.
- Schumann, U., Bugliaro, L., Dörnbrack, A., Baumann, R., and Voigt, C.: Aviation Contrail Cirrus and Radiative Forcing Over Europe During 6 Months of COVID-19, *Geophys. Res. Lett.*, 48, e2021GL092 771, <https://doi.org/10.1029/2021GL092771>, e2021GL092771 2021GL092771, 2021a.
- 305 Schumann, U., Poll, I., Teoh, R., Koelle, R., Spinielli, E., Molloy, J., Koudis, G. S., Baumann, R., Bugliaro, L., Stettler, M., and Voigt, C.: Air traffic and contrail changes over Europe during COVID-19: a model study, *Atmos. Chem. Phys.*, 21, 7429–7450, <https://doi.org/10.5194/acp-21-7429-2021>, accepted, 2021b.
- Unterstrasser, S.: Properties of young contrails – a parametrisation based on large-eddy simulations, *Atmos. Chem. Phys.*, 16, 2059–2082, <https://doi.org/10.5194/acp-16-2059-2016>, 2016.
- 310 Unterstrasser, S. and Gierens, K.: Numerical simulations of contrail-to-cirrus transition – Part 2: Impact of initial ice crystal number, radiation, stratification, secondary nucleation and layer depth, *Atmos. Chem. Phys.*, 10, 2037–2051, <https://doi.org/10.5194/acp-10-2037-2010>, 2010.
- Unterstrasser, S. and Görsch, N.: Aircraft-type dependency of contrail evolution, *J. Geophys. Res. Atmos.*, 119, 14,015–14,027, <https://doi.org/10.1002/2014JD022642>, 2014.
- 315 Unterstrasser, S., Gierens, K., Sölch, I., and Lainer, M.: Numerical simulations of homogeneously nucleated natural cirrus and contrail-cirrus. Part 1: How different are they?, *Meteorol. Zeitschrift*, 26, 621–642, <https://doi.org/10.1127/metz/2016/0777>, 2017.
- Vázquez-Navarro, M., Mannstein, H., and Kox, S.: Contrail life cycle and properties from 1 year of MSG/SEVIRI rapid-scan images, *Atmos. Chem. Phys.*, 15, 8739–8749, <https://doi.org/10.5194/acp-15-8739-2015>, 2015.



- 320 Voigt, C., Schumann, U., Jurkat, T., Schaeuble, D., H. S., A. P., Gayet, J.-F., M. K., J. S., S. B., Schmale, J., Jeßberger, P., Hamburger, T.,  
Lichtenstern, M., Scheibe, M., Gourbeyre, C., J. M., Kübbeler, M., Frey, W., and A. D.: In-situ observations of young contrails – overview  
and selected results from the CONCERT campaign, *Atmos. Chem. Phys.*, <https://doi.org/10.5194/acp-10-9039-2010>, 2010.
- Voigt, C., Schumann, U., Jessberger, P., Jurkat, T., Petzold, A., Gayet, J.-F., Krämer, M., Thornberry, T., and Fahey, D. W.: Extinction and  
optical depth of contrails, *Geophys. Res. Lett.*, 38, <https://doi.org/10.1029/2011GL047189>, 2011.
- 325 Voigt, C., Kleine, J., Sauer, D., Moore, R. H., Bräuer, T., Clercq, P. L., Kaufmann, S., Scheibe, M., Jurkat-Witschas, T., Aigner, M., Bauder,  
U., Borrmann, S., Boose, Y., Crosbie, E., Diskin, G. S., DiGangi, J., Hahn, V., Huber, F., Nowak, J. B., Rauch, B., Rapp, M., Robinson, C.,  
Schripp, T., Shook, M., Winstead, E., Ziemba, L., Schlager, H., and Anderson, B. E.: Cleaner burning jet fuels reduce contrail cloudiness,  
*Nature Commun. Earth Environ.*, <https://doi.org/10.1038/s43247-021-00174-y>, 2021.
- Wallace, J. M. and Hobbs, P. V.: *Atmospheric Science*, Elsevier, Amsterdam, 2 edn., 2006.
- 330 Zschoke, A., Scheuermann, S., and Ortner, J.: *High Biofuel Blends in Aviation (HBBA)*, Tech. rep., Deutsch Lufthansa AG and Wehrwis-  
senschaftliches Institut für Werk- und Betriebsstoffe, 2012.